

Journal of Biomedical Optics

BiomedicalOptics.SPIEDigitalLibrary.org

Spatially multiplexed interferometric microscopy with partially coherent illumination

José Ángel Picazo-Bueno
Zeev Zalevsky
Javier García
Carlos Ferreira
Vicente Micó

SPIE.

José Ángel Picazo-Bueno, Zeev Zalevsky, Javier García, Carlos Ferreira, Vicente Micó, "Spatially multiplexed interferometric microscopy with partially coherent illumination," *J. Biomed. Opt.* 21(10), 106007 (2016), doi: 10.1117/1.JBO.21.10.106007.

Spatially multiplexed interferometric microscopy with partially coherent illumination

José Ángel Picazo-Bueno,^a Zeev Zalevsky,^b Javier García,^a Carlos Ferreira,^a and Vicente Micó^{a,*}

^aUniversitat de València, Departamento de Óptica, C/Doctor Moliner 50, Burjassot 46100, Spain

^bBar-Ilan University, Faculty of Engineering, Ramat-Gan 52900, Israel

Abstract. We have recently reported on a simple, low cost, and highly stable way to convert a standard microscope into a holographic one [Opt. Express 22, 14929 (2014)]. The method, named spatially multiplexed interferometric microscopy (SMIM), proposes an off-axis holographic architecture implemented onto a regular (nonholographic) microscope with minimum modifications: the use of coherent illumination and a properly placed and selected one-dimensional diffraction grating. In this contribution, we report on the implementation of partially (temporally reduced) coherent illumination in SMIM as a way to improve quantitative phase imaging. The use of low coherence sources forces the application of phase shifting algorithm instead of off-axis holographic recording to recover the sample's phase information but improves phase reconstruction due to coherence noise reduction. In addition, a less restrictive field of view limitation (1/2) is implemented in comparison with our previously reported scheme (1/3). The proposed modification is experimentally validated in a regular Olympus BX-60 upright microscope considering a wide range of samples (resolution test, microbeads, swine sperm cells, red blood cells, and prostate cancer cells). © 2016 Society of Photo-Optical Instrumentation Engineers (SPIE) [DOI: 10.1117/1.JBO.21.10.106007]

Keywords: holography; microscopy; phase measurement; medical and biological imaging; interference microscopy.

Paper 160286PR received May 3, 2016; accepted for publication Oct. 6, 2016; published online Oct. 27, 2016.

1 Introduction

Digital holographic microscopy (DHM) rises from a combination of classical holography^{1,2} with optical microscopy³ in the digital domain.⁴ DHM avoids the limited resolution imposed by the finite number and size of the pixels in the digital sensor as well as the limited depth of focus in high numerical aperture (NA) lenses. The former because of the microscope lens magnification resulting in less demanding sampling requirements of the digital sensor.⁵ And the latter by allowing three-dimensional (3-D) sample imaging by numerical refocusing of a two-dimensional (2-D) image at different object planes without using any optomechanical movement.⁶ But maybe more significant is its capability to allow visualization of phase samples using a noninvasive (no need for labeling), full-field (nonscanning), real-time (single-frame acquisition), noncontact (no sample damage), and static (no moving components) operating principle.⁷⁻⁹ Due to its versatility, DHM has been successfully applied to real-time quantitative phase contrast imaging,⁷ polarization microscopy imaging,¹⁰ aberration lens compensation,¹¹ particle tracking,¹² 3-D dynamic analysis of cells,¹³ and in so many other disciplines in the fields of biophotonics, life sciences, and medicine.¹⁴⁻¹⁷

DHM layouts typically use laser sources for generating interference fringes in the experimental configuration. However, coherent light is very sensitive to both the microstructure of the sample and any defect or dust in optical paths. As a result, the complex amplitudes interfering at the recording plane are strongly affected by coherent noise. And such coherent noise severely reduces the optical quality of the reconstructed fields.¹⁸ One way to improve image reconstruction is to reduce speckle noise and coherent artifacts by using different strategies

such as digital processing capabilities¹⁹⁻²¹ or by using specific optical components²²⁻²⁴ or by image averaging.²⁵⁻²⁷ Another strategy is to use partially coherent light sources for illuminating the sample.²⁸⁻⁴² Partially coherent illumination allows coherent noise reduction and increased phase resolution in DHM by avoiding multiple reflections and reducing the contribution of coherent artifacts. Due to this, partially coherent illumination has been implemented in DHM²⁸⁻³⁵ as well as in digital in-line holographic microscopy³⁶⁻⁴² layouts.

We have recently reported on a noncomplex way to convert a commercially available standard microscope into a DHM with only minimal modifications.⁴³ The method, named spatially multiplexed interferometric microscopy (SMIM), rises from our previously developed spatially multiplexed common-path interferometric layout tested on an optical table and under super-resolution purposes.⁴⁴⁻⁴⁶ SMIM simply replaces the broadband light source of the conventional microscopy by a laser diode, it leaves a clear region at the input plane for reference beam transmission, and it properly places a one-dimensional (1-D) diffraction grating in the microscope embodiment. With these three minimal modifications, a regular microscope is converted into a holographic one working under off-axis holographic recording.⁴³ However, two main factors limit the proposed SMIM approach. The first relates with the field of view (FOV) restriction imposed by the need to leave a clear transparent region at the input plane for the reference beam transmission. This fact reduces the useful FOV to one-third of the available one without using SMIM but enables phase information availability. And the second one relates to the use of coherent light sources, which produce coherent noise at the reconstructed images.

*Address all correspondence to: Vicente Micó, E-mail: vicente.mico@uv.es

In this contribution, we have avoided both previously noted drawbacks in SMIM by relaxing the FOV limitation (from one-third to one-half) and by minimizing coherent noise effects. The former is achieved by a slightly different optical design of the input plane's spatially multiplexing. And the latter is obtained by replacing the laser diode by a super luminescent diode (SLD) source with a reduced temporal coherence. However, off-axis recording is prevented since the coherence length of the SLD is lower than the optical path mismatch between both interferometric beams when considering off-axis configuration at SMIM.⁴³ As a consequence, quasi on-axis (or slightly off-axis) holographic recording⁴⁷⁻⁴⁹ with temporal phase-shifting algorithm⁵⁰⁻⁵² is adopted to retrieve quantitative phase-resolved information of the sample.

SMIM is closely related with those methods implemented in regular microscopes to provide quantitative phase imaging. Diffraction phase microscopy (DPM),⁵³ quadriwave lateral shearing interferometry (QLSI),⁵⁴ and Michelson interferometer layout (MIL)⁵⁵ are some examples. In few words, DPM proposes common-path architecture based on splitting into two the imaging beam and synthesizes a reference beam from one of those two beams using spatial filtering with a pinhole; then, both coherent beams are overlapped at the recording CCD plane in off-axis configuration. SMIM differs from DPM in that there is no need to add a pinhole mask at any specific location of the setup to generate the reference beam since it is transmitted by saving a clear area at the input plane. QLSI proposes phase imaging using wavefront sensing implemented with the aid of a modified Hartmann mask. QLSI is a completely different concept approach based on digital wavefront sensing and not in holography. And MIL uses a Michelson layout at the image space to perform off-axis holographic recording at the CCD plane. MIL is based on the fact that the surrounding area of the cell to be imaged is blank so holographic recording using an almost clean reference beam is produced. In other words, MIL needs sparse samples. SMIM differs to MIL since samples can be dense: the only requirement is they will be placed in a restricted area allowing clear reference beam transmission.

The paper is organized as follows. Section 2 provides a layout description of the proposed working scheme highlighting the main difference with respect to Ref. 43. Section 3 experimentally validates SMIM with SLD illumination in a regular microscope (Olympus BX-60) first with synthetic samples (USAF, United States Air Force resolution test target, and microbeads) for calibration purposes and second with complex biosamples [red blood cells (RBC), swine sperm (SS) cells, and prostate cancer (PC-3) cells] for two different objectives (10× and 20×). Sec. 4 concludes the paper.

2 Experimental Layout Considerations

SMIM was previously implemented using the embodiment of a BX60 Olympus upright microscope where three modifications were introduced.⁴³ The first involves the use of coherent illumination for the interferometric recording. This is accomplished in Ref. 43 by using a commercial grade laser diode. The second one defines a specific spatial multiplexing at the input plane for reference and imaging beam transmission in common-path configuration. Note that by spatial multiplexing we mean that a specific spatial distribution needs to be implemented for allowing the transmission at once of both interferometric beams. The spatial multiplexing included in Ref. 43 divides the input plane's FOV into three contiguous areas having the

same width where one is for the sample, another is for the reference beam and the third is blocked. And the third modification inserts a 1-D diffraction grating for mixing both interferometric beams at the recording plane. The 1-D grating is placed at the analyzer insertion slot just before the tube lens system included in the observation tube of the microscope and it allows off-axis holographic recording at the CCD plane. All together it confers the microscope with the capability of quantitative phase imaging by using conventional image processing tools involving digital fast Fourier transform (FFT), spatial filtering, and inverse FFT operation. The experimental validation was presented using a USAF resolution test target as well as RBCs and SS cells.

Now, some modifications are provided for the basic SMIM layout for improving quantitative phase imaging and FOV. The proposed setup is presented in Fig. 1 and it resembles the one included in Fig. 1 of Ref. 43, but with the following three differences. First, the coherent light source, which is externally inserted just below the microscope's XY translation stage, is not a laser diode but an SLD source. SLDs combine the advantages of both light-emitting diode (LED) and laser diode sources since, on one hand, SLDs provide temporal incoherent illumination incoming from a broadband spectrum (such as LEDs) and, on the other hand, SLDs are similar in geometry to laser diodes but without optical feedback mechanism for laser light emission thus providing a high degree of spatial coherence. As result, SLDs provide partially coherent (temporal incoherence) quasipoint illumination that reduces noise incoming from speckle and coherent artifacts while allows interference according to its coherent length⁵⁶ that can be calculated as $L_c = k \lambda^2 / \Delta\lambda \cong 50 \mu\text{m}$, being $k = 0.66$ for Gaussian spectrum, and $\lambda = 650 \text{ nm}$ the central wavelength, and $\Delta\lambda = 6 \text{ nm}$ the spectral bandwidth for the SLD used in the experiments.

Second, the spatial multiplexing at the input plane does not divide the FOV into three regions but only into two ones. This fact improves the useful FOV from one-third to one-half or, in other words, it does not restrict the FOV by a factor of 3 but by a factor of 2. Notice that SMIM with only two regions at the input plane was also proposed at Ref. 43; but this possibility was not implemented because the CCD must be laterally shifted to an off-axis position to record the holograms and this fact is intended to modify the microscope exit port. Figure 2 shows for clarity a comparison between the spatial multiplexing included in Ref. 43 [Fig. 2(a)] and the one proposed in this paper [Fig. 2(b)]. In Fig. 2(a), left side, the three regions in which the FOV is separated in Ref. 43 are identified as R-O-X (initials incoming from the reference, the object, and the X-blocking areas, respectively). The O region is on-axis centered while the R and X ones are at the sides of the O region. This FOV multiplexing is imaged and magnified by the microscope system in the form of R'-O'-X' at the output plane. Since the CCD is centered with the optical axis of the microscope embodiment, only the O' region will fall in its sensitive area. But the proper selection of a 1-D diffraction grating allows a displacement between replicas equal to one-third of the FOV [see Fig. 2(a), right side]. So, the three regions R'-O'-X' will perfectly overlap one to each other at the recording plane and the CCD records an off-axis hologram incoming from the addition of the imaging beam (O') and a tilted reference beam (R') which arrives at the CCD plane with a specific off-axis propagation angle. This propagation angle is enough to separate the diffraction orders of the recorded hologram at the Fourier domain and the complex amplitude distribution of the sample

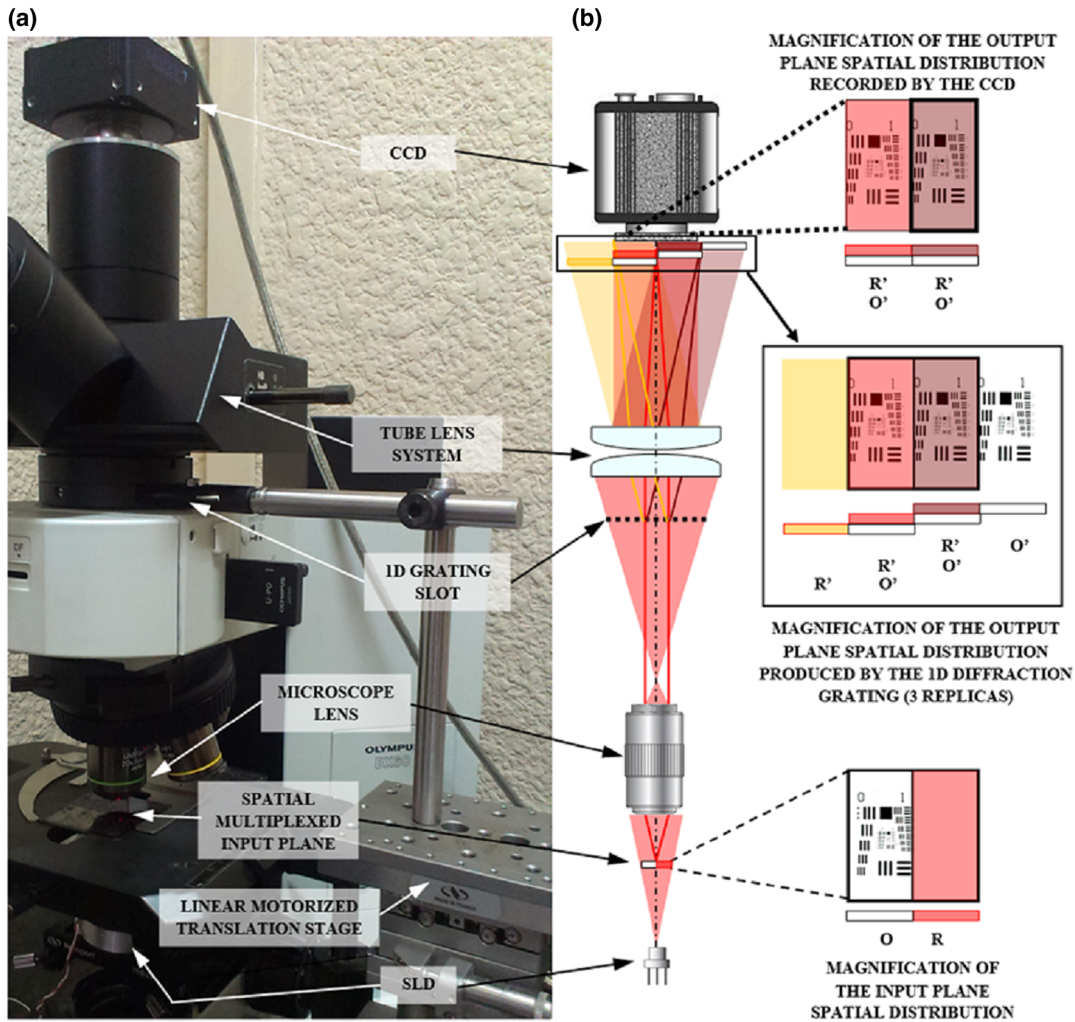


Fig. 1 Picture of (a) the experimental layout and (b) scheme of the proposed SMIM with partially coherent illumination where the main components of SMIM can be identified at both the picture and the scheme. In addition, the spatial multiplexing is included at the input plane, the output plane, and the recorded intensity by the CCD.

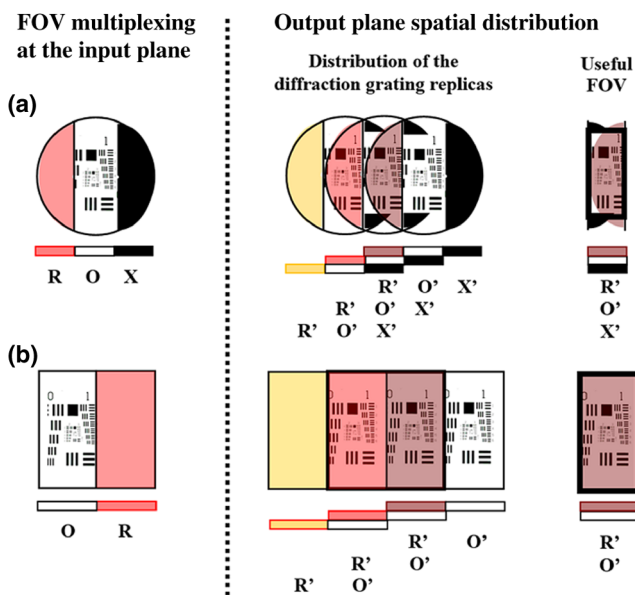


Fig. 2 FOV multiplexing according to the layouts presented in: (a) Ref. 43 and (b) this contribution.

is recovered after conventional digital image processing (FFT, Fourier filtering, and inverse FFT).

The proposed scheme layout [Fig. 2(b), left side] organizes the FOV into two regions where one is used for placing the object (O) and the other for reference beam transmission (R). Thus, by properly selection of the grating's period, overlapping of O' with R' is also provided [Fig. 2(b), right side] and the FOV becomes improved from one-third to one-half of the available one. To compute the grating's basic frequency allowing half of the FOV overlapping, Eq. (7) from Ref. 43 is adapted to the new experimental configuration. In Ref. 43, we proposed a shift of the replicas equal to $2z$ for one-third FOV limitation, being $2z$ the width of the CCD detector. Now and for one-half FOV limitation, the replicas of the grating at the CCD plane must be shifted z . Thus, under the same assumptions as were in Ref. 43 and using Fig. 3, the grating's basic frequency N can be calculated as $N = z/(\lambda f')$, where λ is the illumination wavelength and f' is the focal length of the tube lens (180 mm according to the microscope specifications). Assuming an FOV multiplexing along the shortest CCD direction (as we use in most of the cases), the resulting grating's basic frequency results in $N = 20.64$ linepairs/mm.

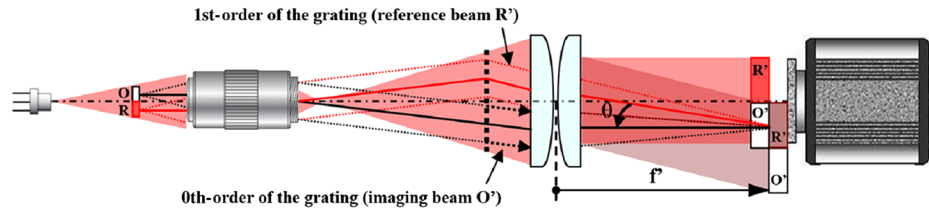


Fig. 3 Scheme of the optical beam paths for calculating mismatches in the optical paths of the reference (red raytracing) and imaging (black raytracing) beams. For clarity, we have removed the yellow raytracing included in Fig. 1 and corresponding with the +1 grating's diffraction order.

Third, and as a consequence of using a partially coherent illumination source, the 1-D diffraction grating must have a larger period than the one used in Ref. 43. Because of the lateral shift of the replicas at the recording plane produced by the 1-D grating, the reference beam optical path is higher than the imaging beam optical path (see Fig. 3). Some rapid calculations will assist with this fact. Assuming that the optical path of both beams is the same until the 1-D diffraction grating and that the grating is closely placed to the tube lens system, the change in optical path between both beams will be produced after passing the tube lens. According to the microscope specifications, the tube lens focal length (f' in Fig. 3) is 180 mm. Thus, while the nondiffracted light (zeroth-order term of the grating) travels 180 mm until reaching the CCD (central ray of the imaging beam included as the black solid ray parallel to the optical axis after the tube lens in Fig. 3), the one of the grating's diffraction orders (central ray of the reference beam included as the red solid ray after the tube lens in Fig. 3) will result in a distance equal to $d = 180 / \cos \theta$, where θ is the tilted beam angle on which the reference beam arrives at the CCD plane. This θ angle is in good approximation the same as the grating's diffraction angle. Considering the 1-D grating used in Ref. 43 with a period of $12.5 \mu\text{m}$ (or 80 lp/mm basic frequency), the θ angle can be calculated from: $\sin \theta = \lambda / p = 0.65 / 12.5 = 0.26$; so the reference beam central ray will travel 186.41 mm until reaching the CCD. The mismatch in optical path is much higher than the coherence length of the SLD source ($50 \mu\text{m}$ as we have previously calculated). So a lower basic frequency diffraction grating must be used. In the experiments, we have used a 20 lp/mm (or $50\text{-}\mu\text{m}$ period) meaning that the diffracted ray will travel 180.015 mm, which is well below the coherence length of the SLD source allowing interferometric recording. But because of this low basic frequency, off-axis holographic recording with spatial filtering in the Fourier domain is prevented and phase-shifting strategy is needed to recover the sample's complex amplitude distribution. Note that, in principle, it is possible to equalize the optical path difference using delay lines in one of the interferometric beams⁵⁷ and, thus, allow single-shot holographic recording with partially coherent sources. But this is not the case for the proposed approach since no real optical path separation happens because of the common-path interferometric architecture.

With these three simple and cost-effective modifications, SMIM implemented in a regular microscope becomes improved as previously stated although some drawbacks also arise. As a general problem in SMIM, the main shortcoming comes from the FOV spatial multiplexing needed to transmit a clear reference beam for the holographic recording. This fact can be fully achieved by designing a specific chamber for the sample. However, the experimental validation included in this paper expands its use to conventional microscope slides, provided

that a clear region will be allocated in side-by-side configuration with the sample. In addition, use of the phase-shifting method presented in this paper yields a double disadvantage when comparing with the previous SMIM technique.⁴³ On the one hand, phase-shifting algorithm prevents the implementation of the technique to samples varying inside the phase-shifting duty cycle. Although this issue can be minimized by a two-step phase-shifting algorithm⁵² and or using additional polarization multiplexing for parallel phase-shifting recordings,^{58,59} it is true that additional restrictions affects the type of samples to be imaged. On the other hand, the microscope embodiment must be equipped with some sort of mechanical stage for grating movement, thus improving the complexity and pricing of the approach. Additional restriction is performed over the retrieved phase values because of the temporal incoherence of the illumination source used in the experiments.

3 Experimental Validation of SMIM with Partially Coherent Illumination

As in Ref. 43, we have used a commercial BX60 Olympus microscope for implementing the modifications involved in SMIM. We have used an SLD source from Exalos (Model EXS6501-B001, 10-mW optical power, 650-nm central wavelength, 6-nm spectral bandwidth) as a partially coherent light source, which is placed just below the manual XY translation stage of the microscope (see Fig. 1). As optics, we have used two different microscope lenses (UMPlanFI) all of them infinity corrected ones: $10\times / 0.30$ NA and $20\times / 0.46$ NA. A Ronchi ruled grating (20 lp/mm period) and a commercial grade CCD camera (Basler A312f, 582×782 pixels, $8.3 \mu\text{m}$ pixel size, 12 bits/pixel) are used as 1-D diffraction grating and imaging device, respectively. The grating is placed on a motorized linear translation stage (Newport, model ESP300) and it is externally introduced in the microscope embodiment in the analyzer insertion slot. We have selected a grating motion step of $2.5 \mu\text{m}$ between consecutive holograms meaning that 20 images integrate a full phase-shifting cycle. In the experiments, we have recorded a total of 40 images, so two full phase-shifting cycles are available. Note that although phase-shifting algorithm can be implemented using a lower number of images, the lower the number the higher the required precision to control the phase step between frames. Thus, a large number of images per cycle have been selected just to minimize uncertainty errors in phase determination but any other phase-shifting algorithm⁵² can be implemented.

3.1 System Calibration Involving Microbeads and a Resolution Target

In this section, we will present the experimental results provided by the proposed method when using the USAF resolution test

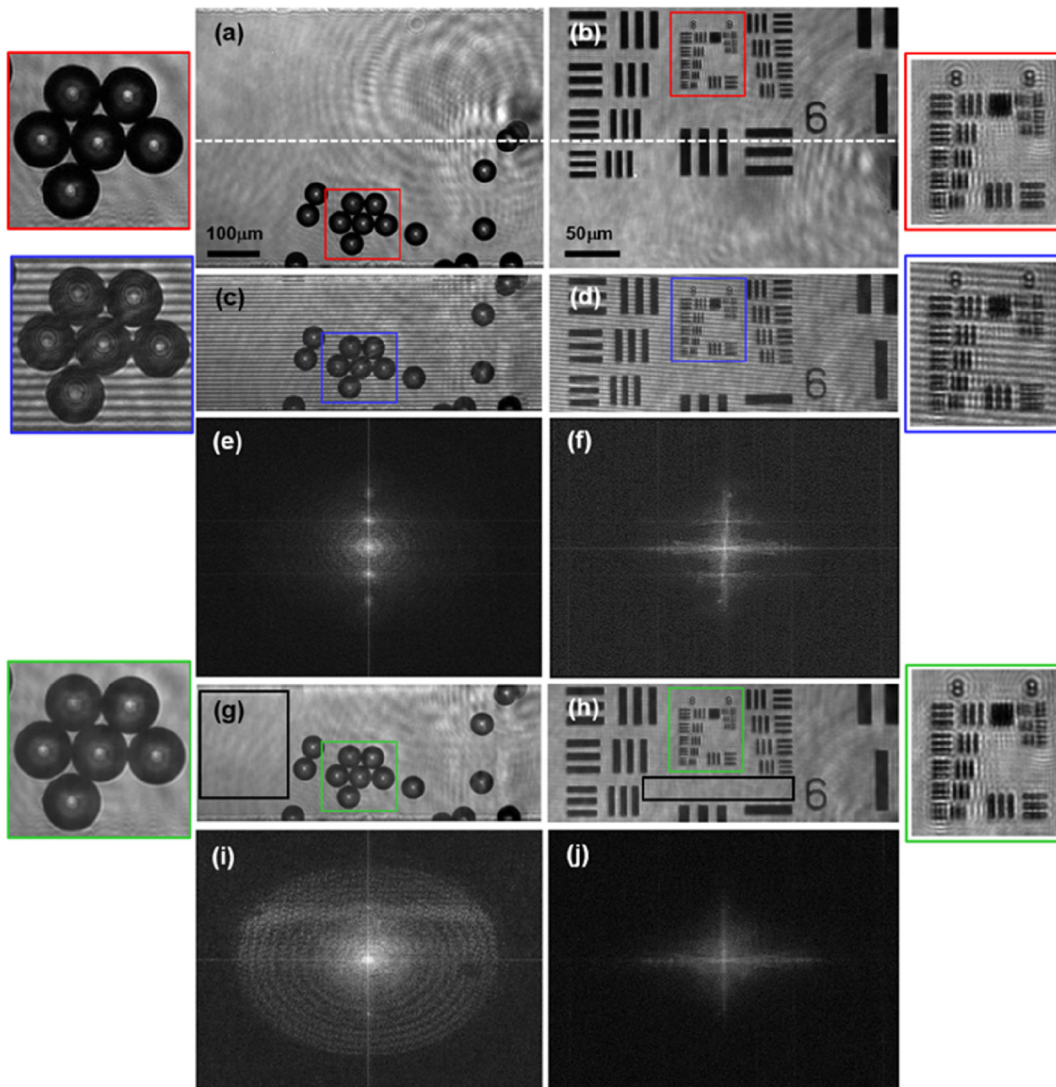


Fig. 4 Experimental results for $10\times/0.30$ NA (left column) and $20\times/0.46$ NA (right column) lenses using microbeads and USAF test, respectively: (a) and (b) the full FOV split by the dashed white lines in the two FOV's spatially multiplexed areas, (c) and (d) a single half FOV frame of the full FOV phase-shifting cycle which can be seen through (Video 1, MOV, 1.5 MB) [URL: <http://dx.doi.org/10.1117/1.JBO.21.10.106007.1>] and (Video 2, MOV, 2.8 MB) [URL: <http://dx.doi.org/10.1117/1.JBO.21.10.106007.2>], (e) and (f) the FFT of the single holograms included in (c) and (d) showing diffraction orders overlapping, (g) and (h) the retrieved images after phase-shifting algorithm implementation, and (i) and (j) the FFT of (g) and (h) showing diffraction order removal.

target and microbeads as input objects. The microbeads (Polybead[®] Microspheres, $45\ \mu\text{m}$ mean diameter) are standard monodisperse polystyrene microspheres in aqueous suspension. The beads are deposited in a conventional microscope slide in sparse mode to assure clear areas in the surroundings of the region containing the microbeads. Regarding the USAF test, we have used the clear area separating groups 4 and 5 from 6 and 7 to pass through it the reference beam.

Figure 4 shows a mosaic of the experimental results obtained for these two types of samples where the microbeads are imaged with the $10\times$ objective and the USAF test by the $20\times$ lens. Figures 4(a) and 4(b) show the direct intensity images provided by the microscope without the grating and where the FOV spatial multiplexing has been marked with a dashed white line (R' in the upper part and O' at the lower one for Figs. 4(a) and viceversa for 4(b), we can see the intensity images of the

interferometric fringes as a consequence of adding the 1-D diffraction grating. To save space, we have included only one-half of the FOV (the one corresponding with the useful O' area). Images presented in Figs. 4(e) and 4(f) include the FFT of a single hologram showing as the hologram's diffraction orders overlap at the Fourier domain as consequence of the slightly off-axis interferometric configuration; so, phase-shifting must be applied to recover the complex amplitude distributions. The whole phase-shifting process is included in two videos for the microbeads (Video 1) and the USAF test (Video 2). The movies correspond with the full set of recorded phase-shifted images where not only the imaging O' area can be seen [as in images included in Figs. 4(c) and (d)] but the full frame also includes the reference R' region. The intensity images obtained after phase-shifting algorithm implementation and the recovered sample's spectrum are included in Figs. 4(g) and 4(h) and 4(i)

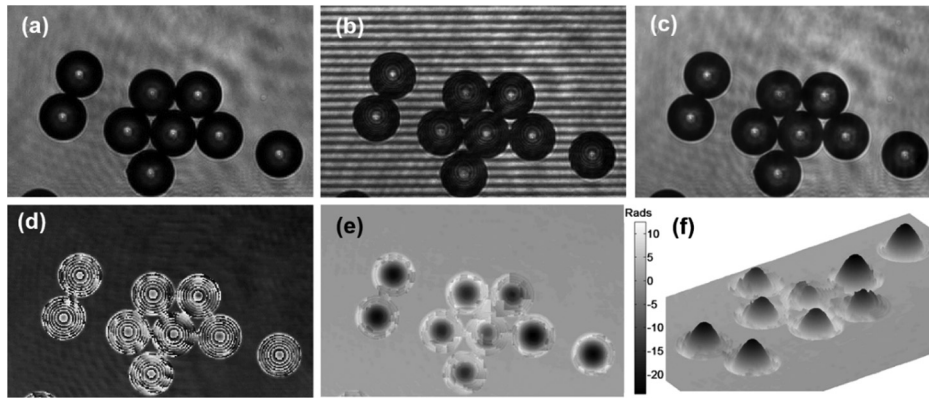


Fig. 5 Experimental results for the $10\times/0.30$ NA objective lens using microbeads: (a–c) magnified images of the intensity distribution retrieved by the proposed method, and (d–f) present the retrieved phase distribution in the form of wrapped, unwrapped, and 3-D view, respectively. Scale bar depicts optical phase in radians and it corresponds with (e) and (f) images.

and 4(j), respectively, where the zeroth- and -first-order terms have been removed. In addition, RGB inner rectangles in Figs. 4(a) and 4(b), 4(c) and 4(d), and 4(g) and 4(h) show in detail a magnification of the inner parts of the images.

Figure 5 includes the experimental results obtained for the microbeads shown in Fig. 4 where only the FOV part containing the microspheres is included. As in Figs. 4(a)–4(c) present the intensity images corresponding with the direct imaging mode

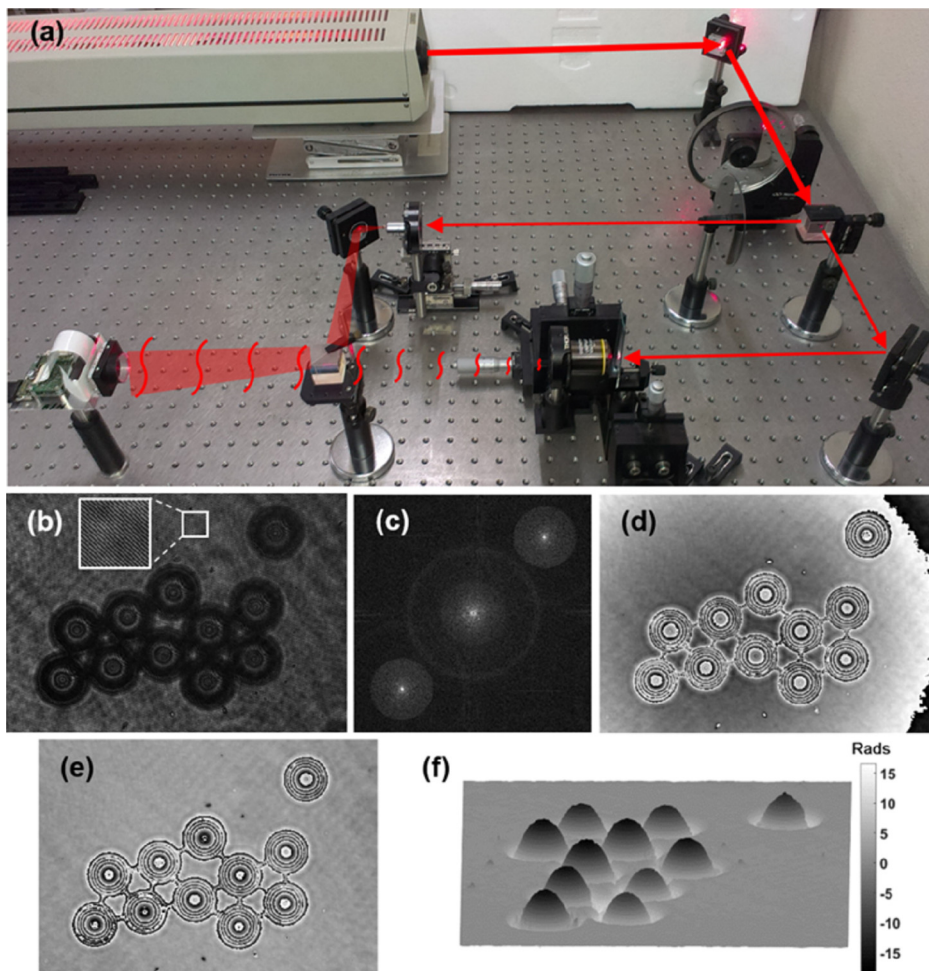


Fig. 6 Experimental results for the $10\times/0.30$ NA objective lens using microbeads in a regular Mach-Zehnder interferometric configuration: (a) the experimental setup, (b) the off-axis recorded hologram, (c) its FFT, (d) the recovered phase distribution after spatial filtering one of the diffraction orders included in (c), (e) the recovered phase distribution after additional spherical and linear digital phase compensation of the image included in (d), and (f) a 3-D unwrapped phase distribution plot of the microbeads. Gray-level scale in (f) represents optical phase in radians.

(no grating in the layout), the interferometric fringes after 1-D grating insertion, and the retrieved image after phase-shifting algorithm, respectively. However, SMIM allows phase recovery and this can be checked with the phase information coming from the microbeads. Figures 4(d)–4(f) include the retrieved wrapped phase distribution, the unwrapped phase distribution, and a 3-D view of the unwrapped phase distribution, respectively.

In order to validate these results, we have assembled a conventional Mach–Zehnder interferometric configuration at the lab. Thus, a direct comparison between quantitative phase values provided by SMIM with partial coherent illumination (Fig. 5) and the obtained ones with a conventional DHM platform (Fig. 6) can be performed. For the DHM implementation, we have used a He–Ne laser as illumination source for imaging the microbeads with the same microscope objective ($10\times/0.30$ NA). The results from DHM are presented in Fig. 6 including the experimental Mach–Zehnder layout at the lab [Fig. 6(a)], the recorded hologram [Fig. 6(b)], its FFT [Fig. 6(c)], the retrieved phase distribution before [Fig. 6(d)] and after [Fig. 6(e)] phase compensation (spherical and linear factors) and unwrapping, and a 3-D view of the unwrapped phase distribution [Fig. 6(f)].

Although the imaged group of microbeads in Fig. 6 is not the same one as in Fig. 5, they are $45\ \mu\text{m}$ spheres so a similar phase profile must be obtained. As one can see by comparing images in Figs. 5(f) and 6(f), the phase delay introduced by the microbeads is almost the same. This fact shows a high concordance between the unwrapped phase values provided by both methods and validates that the quantitative phase information provided by the proposed approach perfectly matches the one provided by conventional holographic methods.

3.2 Experimental Results with Biosamples

Now SMIM with partially coherent illumination is tested using different fixed biological samples. In particular, we have selected RBCs, SS cells, and PC-3 cells. The RBCs were stained onto the microscope slide using a specially prepared mixture of methylene blue and eosin in methanol (Wright stain), the SS cells were unstained but dried up for fixing them on a counting chamber, and the PC-3 cells were *in vivo* cultured and mounted in a microscope slide after centrifugation and resuspension into a cytopreservative solution. As in Ref. 43, we have not built a specially designed chamber for the FOV multiplexing but we are

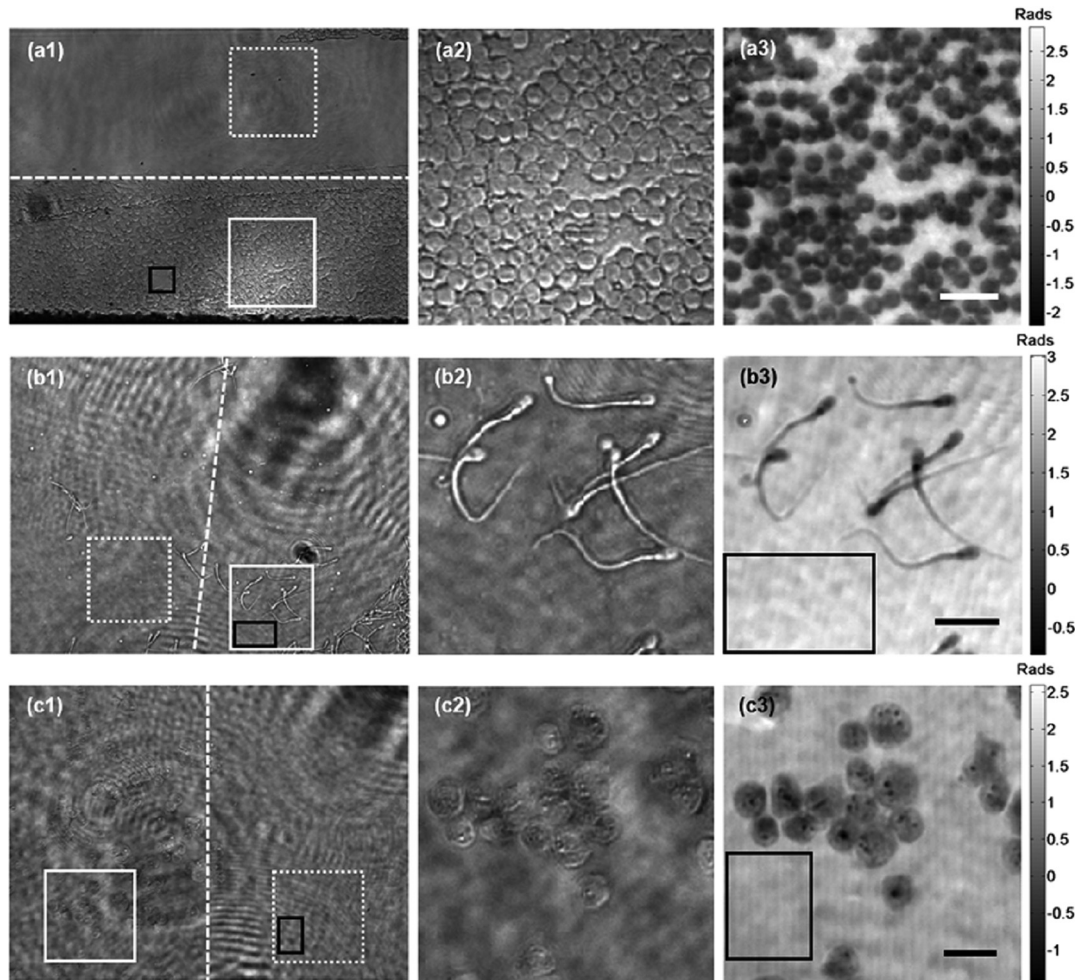


Fig. 7 Experimental results for the $10\times/0.30$ NA microscope lens using biosamples: (a) RBCs, (b) SS cells, and (c) PC-3. Images at left column (1) show the direct intensity image without the grating showing the FOV multiplexed regions. Images at central column (2) present the direct intensity image of the group of cells marked with a solid white line square in (1). And images at right column (3) include the retrieved unwrapped phase distribution using the proposed method. Scale bars: the solid lines at the lower right corner of (a3), (b3), and (c3) represent $25\ \mu\text{m}$.

taking advantage of clear areas in the microscope slide for reference beam transmission.

Figures 7 and 8 include the experimental results for the aforementioned biosamples when using the 10× and the 20× microscope objectives, respectively. The figures are structured in rows (a-b-c) and columns (1-2-3) corresponding with a different biosample and a different image per biosample, respectively. At the left column (1) of both figures, we have included the direct intensity image without grating insertion to identify the spatially multiplexed regions at the input plane. At those images, the dashed white line separates both multiplexed regions (O and R) at the input plane; the solid white line square marks a given region of interest (ROI) including some cells which are magnified on (2) and (3); and the dotted white line square identifies the clear region which will overlap with the cells for SMIM. In addition, note as figures (b1) and (c1) at Fig. 7 include an FOV multiplexing in a different direction. This is because the experimental considerations for those biosamples suggested for us to rotate the CCD at the output port of the microscope for a better implementation of the proposed approach. At the central column (2), we have included the direct intensity image of the cells included in the ROI marked in (1). Finally, the right

column (3) presents the unwrapped phase distribution (positive phase contrast images) retrieved when applying the proposed SMIM method. The gray-scale bars in (3) depict optical phase in radians.

Since SMIM performs holographic recording, the phase information is retrieved; so additional images such as negative phase contrast, DIC in different directions, and 3-D plots can be digitally processed and presented. Figures 9 and 10 include, just as examples, the negative-phase contrast images (2-D and 3-D visualizations) of the positive-phase contrast images included along Figs. 6 and 7 for the three analyzed biosamples.

3.3 SNR Analysis in Spatially Multiplexed Interferometric Microscopy

As a final comparative, we have included an analysis of the standard deviation (STD) of the retrieved phase distributions when using SMIM with off-axis holographic recording⁴³ and the proposed SMIM with partially coherent illumination. STD values are very useful to evaluate spatial noise and image quality in quantitative-phase imaging because it provides a direct value on the phase stability provided by the holographic method. STD

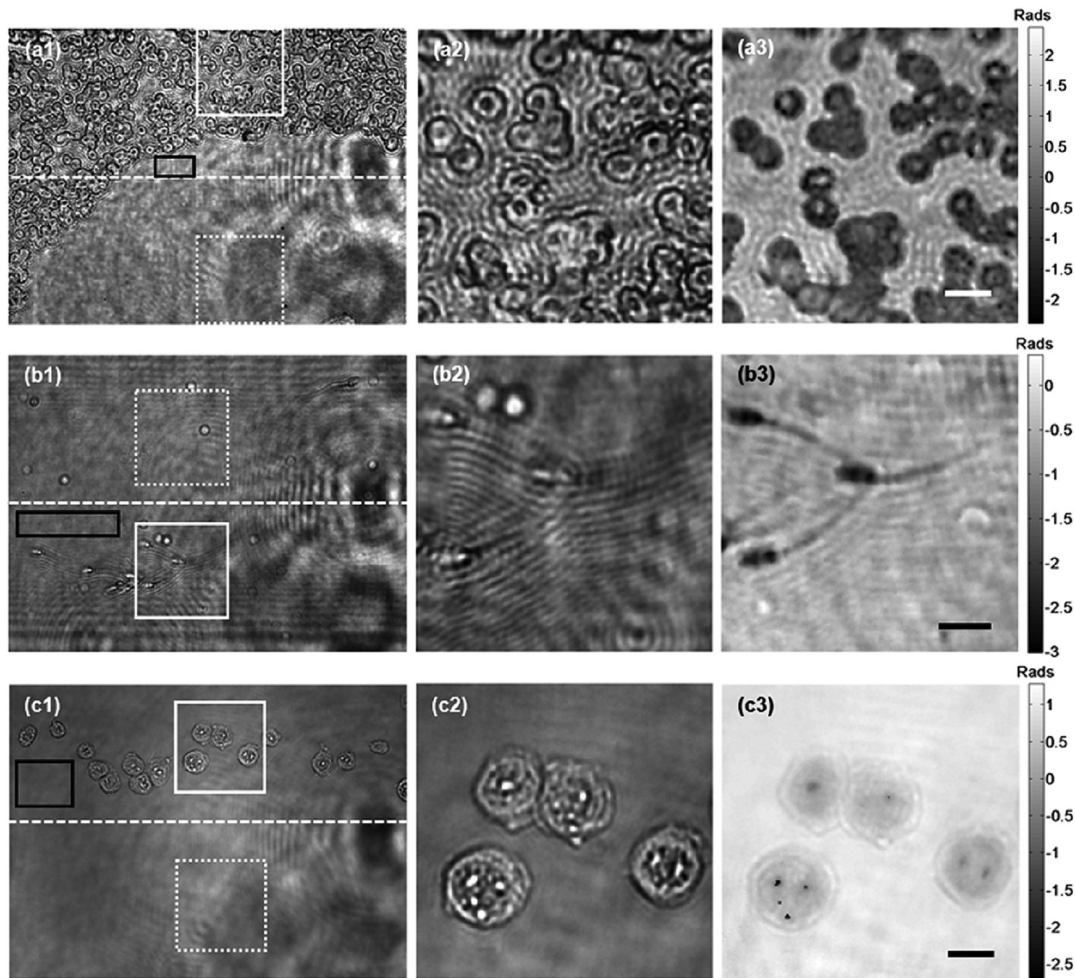


Fig. 8 Experimental results for the 20 × /0.46 NA microscope lens using biosamples: (a) RBCs, (b) SS cells, and (c) PC-3. Images at left column (1) show a direct image without the grating showing the FOV multiplexed regions. Images at central column (2) present the direct intensity image of the group of cells marked with a solid white line square in (1). And images at right column (3) include the retrieved unwrapped phase distribution using the proposed method. Scale bars: the solid lines at the lower right corner of (a3), (b3), and (c3) represent 10 μm .

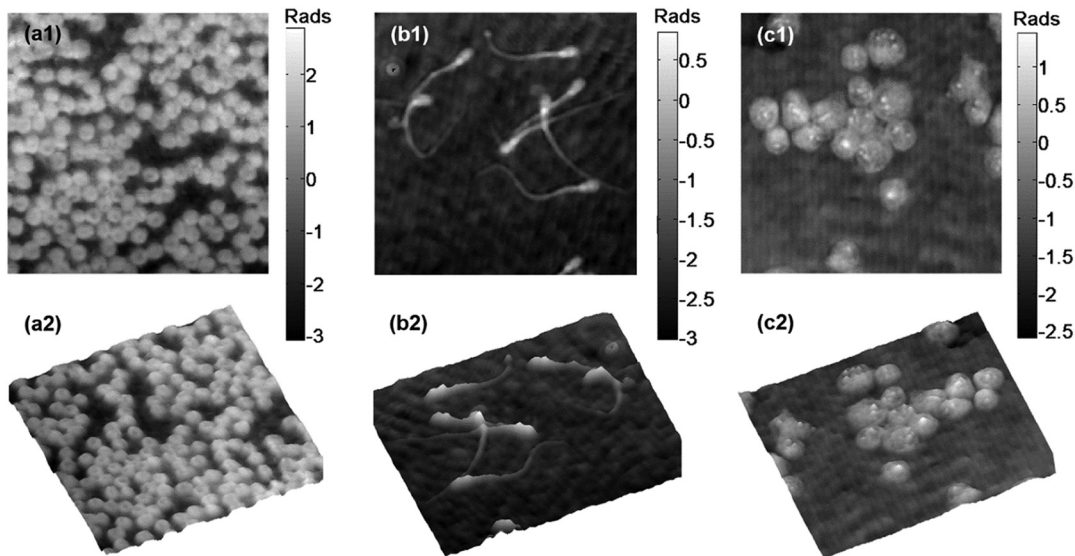


Fig. 9 Experimental results for the $10\times/0.30$ NA microscope lens using biosamples: (a) RBCs, (b) SS cells, and (c) PC-3. Images in upper row (1) are the negative-phase contrast images of the ones included in Figs. 7(a3), 7(b3), and 7(c3), respectively, while the ones included in the lower row (2) include the 3-D representations of the negative-phase contrast images. Scales are equal to the images included in Fig. 7.

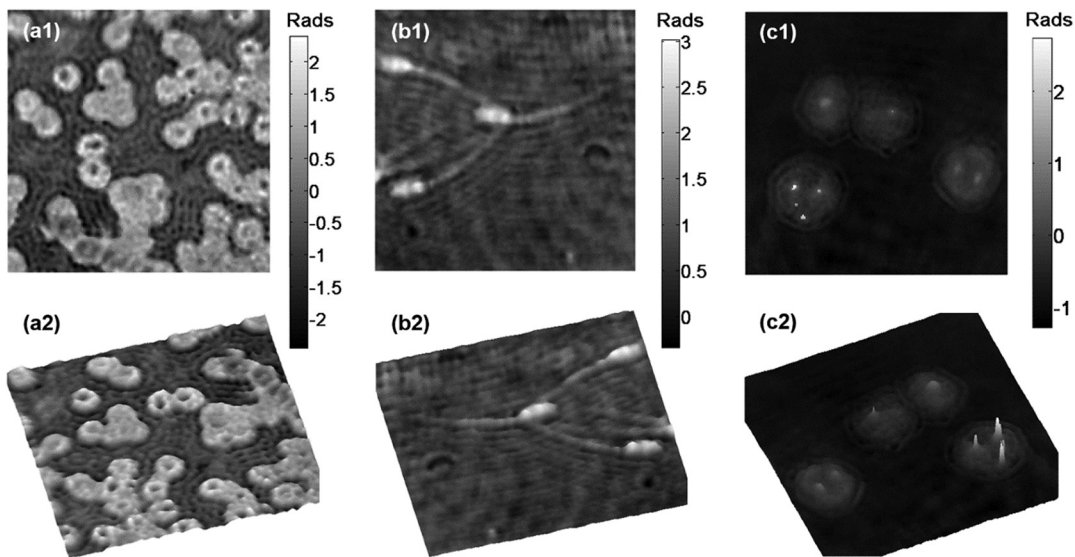


Fig. 10 Experimental results for the $20\times/0.46$ NA microscope lens using biosamples: (a) RBCs, (b) SS cells, and (c) PC-3. Images in upper row (1) are the negative-phase contrast images of the ones included in Figs. 8(a3), 8(b3), and 8(c3), respectively, while the ones included in the lower row (2) include the 3-D representations of the negative-phase contrast images. Scales are equal to the images included in Fig. 8.

values are computed over some of the clear regions (background of the image) available at the retrieved phase distribution. STD is respectively computed from a single hologram and from the image resulting when considering the whole set (40 frames and 2 cycles) of temporally phase-shifted holograms for the cases of SMIM in off-axis configuration⁴³ and the proposed method. In the case of the proposed method, the clear area for computing the STD value is included in Fig. 4. To allow the comparative, we have selected the USAF test images since it is the unique object tested at both in Ref. 43 and in the actual paper with the same microscope objective ($20\times/0.46$ NA lens). Note that although an SS sample is also included in Ref. 43 and here, the

counting chamber is different so the expected STD values will not be useful for direct comparison. Thus, the STD values for the USAF using SMIM with off-axis configuration⁴³ and with partially coherent sources are 0.31 and 0.033 rad, respectively. These values provide an improvement factor close to 10 in phase quality reconstruction as consequence of using partially coherent illumination.

In addition and for completeness, we have computed the STD values of all the retrieved images presented in this contribution. The selected clear areas for STD computation are marked with black rectangles in Figs. 4(g), 7, and 8. Note that we have selected clear areas far away from the parasitic

Table 1 STD analysis in SMIM with partially coherent illumination.

	Microbeads	RBCs	SS cells	PC-3
10 × /0.30 NA STD (rad)	0.026	0.027	0.026	0.032
20 × /0.46 NA STD (rad)	No data	0.06	0.028	0.025

noise due to internal dirt introduced by the illumination and this areas are sometimes inside the magnified region while other not. Results are summarized in Table 1. One can see that the background fluctuation of the retrieved phase using SMIM with partially coherent illumination is highly stable and in the order of $1/10^{\text{th}}$ of the phase stability provided by SMIM in Ref. 43.

4 Conclusions

We have presented a modification of our previously reported SMIM method⁴³ with improved capabilities from a quantitative phase imaging reconstruction point of view but with some penalizations when considering its applicability (slightly more complex hardware modification and useless for dynamic samples). SMIM proposes a noncomplex, low cost, and highly stable way to convert a standard microscope into a holographic one. SMIM is based on a CPI architecture using input plane spatial multiplexing and a 1-D diffraction grating to allow holographic recording. SMIM was previously validated as demonstrator at the lab^{44–46} and implemented in a regular microscope.⁴³ In the latter validation, SMIM allows holographic imaging in a regular microscope by three small modifications: a coherent illumination source, a 1-D diffraction grating, and a specific input plane spatial distribution. The holographic recording is performed in off-axis configuration and reconstruction is achieved by spatial filtering at the Fourier domain. SMIM was validated for different samples and objectives showing a useful FOV of one-third of the available one.

In this contribution, SMIM has been validated using a partially (temporally reduced) coherent source, with a less restrictive FOV limitation (one-half instead of one-third), and for different samples and objectives. As a consequence of the reduced temporal coherence of the illumination, phase information is retrieved by phase-shifting algorithm meaning that the sample must be static during the recording time (typically a few seconds). However, spatial phase noise becomes improved and phase images show better image quality in reconstruction. The proposed SMIM modification is aimed for those cases where improved SNR and FOV will be more important issues than real time. Moreover, the use of temporally reduced coherence sources is of particular significance when implementing DHM with commercially available objectives and microscope embodiments containing a lot of glass–air interfaces without specific coatings for the used wavelength, thus generating several back reflections that can result in parasitic interference patterns. The experimental results for synthetic objects (USAF test and microbeads) as well as static biosamples (RBCs, SS cells, and PC-3) verify these assumptions. Future work will be focused on implementing the proposed technique into an inverted microscope and apply it for the analysis of live specimens using partially coherent illumination with equalized optical path difference, i.e., using a single illumination shot.

Acknowledgments

We want to thank Prof. Carles Soler and Mr. Paco Blasco from Proiser R+D S.L. for providing the swine sperm sample and Dr. José Antonio López-Guerrero from Fundación Instituto Valenciano de Oncología - FIVO for PC-3 biosample preparation. Also, part of this work has been funded by the Spanish Ministerio de Economía y Competitividad and the Fondo Europeo de Desarrollo Regional (FEDER) under the project FIS2013-47548-P.

References

1. D. Gabor, "A new microscopic principle," *Nature* **161**, 777–778 (1948).
2. G. L. Rogers, "Experiments in diffraction microscopy," *Proc. R. Soc. Edinburgh A* **63**, 193–221 (1952).
3. D. Gabor and W. P. Goss, "Interference microscope with total wavefront reconstruction," *J. Opt. Soc. Am.* **56**, 849–856 (1966).
4. J. W. Goodman and R. W. Lawrence, "Digital image formation from electronically detected holograms," *Appl. Phys. Lett.* **11**, 77–79 (1967).
5. E. Cuche, P. Marquet, and C. Depeursinge, "Simultaneous amplitude-contrast and quantitative phase-contrast microscopy by numerical reconstruction of Fresnel off-axis holograms," *Appl. Opt.* **38**, 6994–7001 (1999).
6. P. Ferraro et al., "Extended focused image in microscopy by digital holography," *Opt. Express* **13**, 6738–6749 (2005).
7. P. Marquet et al., "Digital holographic microscopy: a noninvasive contrast imaging technique allowing quantitative visualization of living cells with subwavelength axial accuracy," *Opt. Lett.* **30**, 468–470 (2005).
8. B. Kemper and G. von Bally, "Digital holographic microscopy for live cell applications and technical inspection," *Appl. Opt.* **47**, A52–A61 (2008).
9. M. K. Kim, "Principles and techniques of digital holographic microscopy," *SPIE Rev.* **1**, 018005 (2010).
10. T. Colomb et al., "Polarization microscopy by use of digital holography: application to optical-fiber birefringence measurements," *Appl. Opt.* **44**, 4461–4469 (2005).
11. P. Ferraro et al., "Compensation of the inherent wave front curvature in digital holographic coherent microscopy for quantitative phase-contrast imaging," *Appl. Opt.* **42**, 1938–1946 (2003).
12. J. Sheng, E. Malkiel, and J. Katz, "Digital holographic microscope for measuring three-dimensional particle distributions and motions," *Appl. Opt.* **45**, 3893–3901 (2006).
13. F. Dubois et al., "Digital holographic microscopy for the three-dimensional dynamic analysis of in vitro cancer cell migration," *J. Biomed. Opt.* **11**, 054032 (2006).
14. G. von Bally, *Holography in Medicine and Biology*, Springer, Berlin (1979).
15. M. K. Kim, *Digital Holographic Microscopy: Principles, Techniques, and Applications*, 1st ed., Springer, New York (2011).
16. N. T. Shaked, Z. Zalevsky, and L. L. Satterwhite, Eds., *Biomedical Optical Phase Microscopy and Nanoscopy*, Academic Press, Oxford (2012).
17. C. Mann et al., "High-resolution quantitative phase-contrast microscopy by digital holography," *Opt. Express* **13**, 8693–8698 (2005).
18. P. Chavel, "Optical noise and temporal coherence," *J. Opt. Soc. Am.* **70**, 935–943 (1980).
19. Y. Frauel et al., "Distortion-tolerant three-dimensional object recognition with digital holography," *Appl. Opt.* **40**, 3887–3893 (2001).
20. A. Ozcan et al., "Speckle reduction in optical coherence tomography images using digital filtering," *J. Opt. Soc. Am. A* **24**, 1901–1910 (2007).
21. V. Bianco et al., "Random resampling masks: a non-Bayesian one-shot strategy for noise reduction in digital holography," *Opt. Lett.* **38**, 619–621 (2013).
22. I. Moon and B. Javidi, "Three-dimensional speckle-noise reduction by using coherent integral imaging," *Opt. Lett.* **34**, 1246–1248 (2009).
23. S. Kubota and J. W. Goodman, "Very efficient speckle contrast reduction realized by moving diffuser device," *Appl. Opt.* **49**, 4385–4391 (2010).
24. G. Ouyang et al., "Speckle reduction using a motionless diffractive optical element," *Opt. Lett.* **35**, 2852–2854 (2010).

25. T. Baumbach et al., "Improvement of accuracy in digital holography by use of multiple holograms," *Appl. Opt.* **45**, 6077–6085 (2006).
26. V. Micó, C. Ferreira, and J. García, "Surpassing digital holography limits by lensless object scanning holography," *Opt. Express* **20**, 9382–9395 (2012).
27. V. Micó, C. Ferreira, and J. García, "Lensless object scanning holography for two-dimensional mirror-like and diffuse reflective objects," *Appl. Opt.* **52**, 6390–6400 (2013).
28. F. Dubois, L. Joannes, and J.-C. Legros, "Improved three-dimensional imaging with a digital holography microscope with a source of partial spatial coherence," *Appl. Opt.* **38**, 7085–7094 (1999).
29. F. Dubois et al., "Partial spatial coherence effects in digital holographic microscopy with a laser source," *Appl. Opt.* **43**, 1131–1139 (2004).
30. F. Dubois et al., "Digital holographic microscopy with reduced spatial coherence for three-dimensional particle flow analysis," *Appl. Opt.* **45**, 864–871 (2006).
31. B. Kemper et al., "Characterisation of light emitting diodes (LEDs) for application in digital holographic microscopy for inspection of micro and nanostructured surfaces," *Opt. Las. Eng.* **46**, 499–507 (2008).
32. C. Remmersmann et al., "Phase noise optimization in temporal phase-shifting digital holography with partial coherence light sources and its application in quantitative cell imaging," *Appl. Opt.* **48**, 1463–1472 (2009).
33. P. Kolman and R. Chmelík, "Coherence-controlled holographic microscope," *Opt. Express* **18**, 21990–22003 (2010).
34. F. Dubois and C. Yourassowsky, "Full off-axis red-green-blue digital holographic microscope with LED illumination," *Opt. Lett.* **37**, 2190–2192 (2012).
35. T. Slabý et al., "Off-axis setup taking full advantage of incoherent illumination in coherence-controlled holographic microscope," *Opt. Express* **21**, 14747–14762 (2013).
36. L. Repetto, E. Piano, and C. Pontiggia, "Lensless digital holographic microscope with light-emitting diode illumination," *Opt. Lett.* **29**, 1132–1134 (2004).
37. W. Bishara et al., "Lensfree on-chip microscopy over a wide field-of-view using pixel super-resolution," *Opt. Express* **18**, 11181–11191 (2010).
38. G. Biener et al., "Combined reflection and transmission microscope for telemedicine applications in field settings," *Lab Chip* **11**, 2738–2743 (2011).
39. I. P. Ryle, S. McDonnell, and J. T. Sheridan, "Lensless multispectral digital in-line holographic microscope," *J. Biomed. Opt.* **16**, 126004 (2011).
40. P. Petruck, R. Riesenberger, and R. Kowarschik, "Partially coherent light-emitting diode illumination for video-rate in-line holographic microscopy," *Appl. Opt.* **51**, 2333–2340 (2012).
41. T. Pitkääho, M. Niemelä, and V. Pitkääkangas, "Partially coherent digital in-line holographic microscopy in characterization of a microscopic target," *Appl. Opt.* **53**, 3233–3240 (2014).
42. B. Perucho and V. Micó, "Wavefront hologscopy: application of digital in-line holography for the inspection of engraved marks in progressive addition lenses," *J. Biomed. Opt.* **19**, 016017 (2014).
43. V. Mico et al., "Spatially-multiplexed interferometric microscopy (SMIM): converting a standard microscope into a holographic one," *Opt. Express* **22**, 14929–14943 (2014).
44. V. Mico, Z. Zalevsky, and J. García, "Super-resolution optical system by common-path interferometry," *Opt. Express* **14**, 5168–5177 (2006).
45. V. Mico, Z. Zalevsky, and J. García, "Common-path phase-shifting digital holographic microscopy: a way to quantitative imaging and super-resolution," *Opt. Commun.* **281**, 4273–4281 (2008).
46. V. Mico, J. García, and Z. Zalevsky, "Quantitative phase imaging by common-path interferometric microscopy: application to super-resolved imaging and nanophotonics," *J. Nanophoton* **3**, 031780 (2009).
47. P. Gao et al., "Parallel two-step phase-shifting digital holograph microscopy based on a grating pair," *J. Opt. Soc. Am. A* **28**, 434–440 (2011).
48. P. Gao et al., "Parallel two-step phase-shifting point-diffraction interferometry for microscopy based on a pair of cube beamsplitters," *Opt. Express* **19**, 1930–1935 (2011).
49. M. Shan et al., "Parallel two-step spatial carrier phase-shifting common-path interferometer with a Ronchi grating outside the Fourier plane," *Opt. Express* **21**, 2126–2132 (2013).
50. I. Yamaguchi and T. Zhang, "Phase-shifting digital holography," *Opt. Lett.* **22**, 1268–1270 (1997).
51. T. Zhang and I. Yamaguchi, "Three-dimensional microscopy with phase-shifting digital holography," *Opt. Lett.* **23**, 1221–1223 (1998).
52. T. Kreis, *Handbook of Holographic Interferometry: Optical and Digital Methods*, Wiley-VCH Verlag GmbH & Co. KGaA, Weinheim (2005).
53. G. Popescu et al., "Diffraction phase microscopy for quantifying cell structure and dynamics," *Opt. Lett.* **31**, 775–777 (2006).
54. P. Bon et al., "Quadriwave lateral shearing interferometry for quantitative phase microscopy of living cells," *Opt. Express* **17**, 13080–13094 (2009).
55. B. Kemper et al., "Simplified approach for quantitative digital holographic phase contrast imaging of living cells," *J. Biomed. Opt.* **16**, 026014 (2011).
56. M. Born and E. Wolf, *Principles of Optics*, 7th ed., Cambridge University, Cambridge, UK (1999).
57. P. Langehanenberg, G. V. Bally, and B. Kemper, "Application of partially coherent light in live cell imaging with digital holographic microscopy," *J. Mod. Opt.* **57**, 709–717 (2010).
58. Y. Awatsuji, M. Sasada, and T. Kubota, "Parallel quasi-phase-shifting digital holography," *Appl. Phys. Lett.* **85**, 1069–1071 (2004).
59. T. Tahara et al., "Parallel phase-shifting digital holographic microscopy," *Biomed. Opt. Express* **1**, 610–616 (2010).

Biographies for the authors are not available.